

# An Indirect Model Predictive Control for Matrix Converters

Baiqi Dai

Dept. of Electrical, Electronic,  
Telecommunications Engineering  
and Naval Architecture  
University of Genova  
Genova, Italy  
baiqi.dai@edu.unige.it

Massimiliano Passalacqua

Dept. of Electrical, Electronic,  
Telecommunications Engineering  
and Naval Architecture  
University of Genova  
Genova, Italy  
massimiliano.passalacqua@unige.it

Petros Karamanakos

Faculty of Information Technology  
and Communication Sciences  
Tampere University  
Tampere, Finland  
p.karamanakos@ieee.org

Andrea Formentini

Dept. of Electrical, Electronic, Telecommunications  
Engineering and Naval Architecture  
University of Genova  
Genova, Italy  
andrea.formentini@unige.it

Mario Marchesoni

Dept. of Electrical, Electronic, Telecommunications  
Engineering and Naval Architecture  
University of Genova  
Genova, Italy  
marchesoni@unige.it

**Abstract**—This paper proposes an indirect model predictive control (MPC) approach for matrix converters. This approach maintains a fixed switching frequency and achieves a low harmonic distortion in both the voltage and current, thereby overcoming the main limitations of conventional direct MPC. More importantly, the proposed strategy improves the stability margin and control bandwidth compared to conventional proportional-integral (PI)-based linear controllers. Consequently, the output current of the converter—and thus its power—can be increased, enabling more effective utilization of the hardware. To verify these findings, the proposed indirect MPC scheme is implemented on a low-cost control platform operating at a 10 kHz sampling frequency. The presented results demonstrate that the required computation time of approximately 50  $\mu$ s, when a three-step horizon is considered, is well within the capabilities of the chosen platform, confirming its real-time feasibility.

**Index Terms**—Model predictive control, matrix converter, indirect control, control bandwidth, stability margin.

## I. INTRODUCTION

The matrix converter (MC) is an alternative topology to the three-phase (3 $\Phi$ ) ac-ac back-to-back converter [1], [2]. It offers a more compact design by eliminating the need for an intermediate dc-link capacitor or inductor [3], as illustrated in Fig. 1. However, the resonance introduced by the  $LC$  input filter presents a challenge in designing a high-bandwidth, stable controller [4].

To address this challenge and enhance system stability, the conventional approach typically involves using a digital filter for the input voltage measurement in combination with a proportional-integral (PI) controller [5]. For the linear PI controller, control theory provides well-established methods for theoretical stability analysis. For instance, small-signal stability analysis [6], impedance ratio criterion [7], and large-signal stability analysis [8] have been applied to investigate the

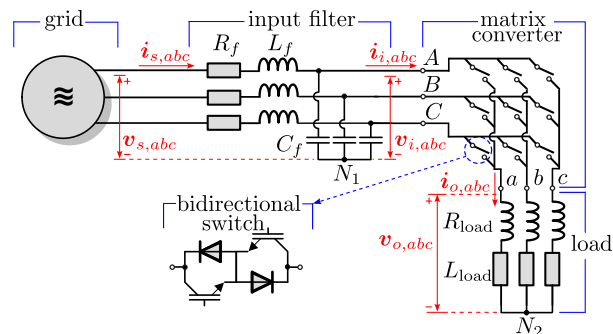


Fig. 1: A grid-connected matrix converter with a  $RL$  load.

resonance issue. However, PI-based control solutions suffer from limited bandwidth because of the inherent trade-off between stability and dynamic response, which ultimately constrains overall system performance.

In contrast, model predictive control (MPC) has demonstrated the ability to enhance closed-loop stability while maintaining high bandwidth, owing to its multiple-input multiple-output (MIMO) nature and the use of full-state information in the prediction process [9]–[11]. Consequently, MPC has been applied to matrix converters with promising results [12], [13]. Among its variants, direct MPC—i.e., MPC without a dedicated modulator—is the most widely adopted, particularly in the form of an output-reference tracking control scheme, known as finite control set MPC (FCS-MPC) [14].

However, two main challenges hinder the practical deployment of direct MPC for matrix converters. First, similar to PI-based control, direct MPC must address the resonance introduced by the input filter. To mitigate this issue, active

damping techniques have been proposed [15]. Nevertheless, these methods add complexity to the tuning process, which often relies on empirical trial-and-error adjustments. Second, the absence of a dedicated modulation stage in direct MPC results in a variable switching frequency. This can potentially lead to high ripple in the output current and voltage of the converter, rendering direct MPC unsuitable for applications requiring low harmonic distortion. To overcome this limitation, a modulated model predictive control (M2PC) strategy was proposed to achieve a fixed switching frequency [16]. However, this approach still produces lower current quality compared to PI-based controllers.

Considering the limitations of both conventional PI-based control and direct MPC, this paper proposes an indirect MPC strategy for matrix converters, i.e., an MPC approach that incorporates a dedicated modulation stage [17]. The proposed method achieves a favorable trade-off between stability and bandwidth, thereby overcoming the restrictions of conventional PI controllers. Furthermore, it guarantees a fixed switching frequency and reduces current and voltage ripple. A key feature of the proposed scheme is that the optimization problem underlying indirect MPC is formulated as a constrained quadratic program (QP), resulting in a moderate computational burden. This enables the real-time implementation of the proposed MPC strategy on a low-cost control platform. Experimental results obtained from a custom-built prototype validate the effectiveness of the proposed control strategy.

## II. SYSTEM MODELING AND MPC DESIGN

This section outlines the design of the proposed MPC strategy. This consists of the following five steps, while the block diagram is provided in Fig. 2.

A) Modeling of the system using circuit theory and representation in a nonlinear state-space form.

B) Computation of the reference values<sup>1</sup> for the state  $\mathbf{x}$  and control input  $\mathbf{u}$ .

C) Linearization of the nonlinear system around the operating point defined by the references, followed by the derivation of the linear state-space model in the continuous-time domain and, subsequently, in the discrete-time domain.

D) Formulation of a cost function based on the chosen control objectives, and subsequent design of the optimal control problem.

E) Implementation of a real-time solver to efficiently solve the constrained QP underlying indirect MPC.

### A. System Modeling

With reference to Fig. 1, the average model of an MC in the synchronously rotating ( $dq$ ) reference frame can be derived as shown in [18], and it is expressed as<sup>2</sup>

$$\frac{d\mathbf{x}(t)}{dt} = \mathbf{f}(\mathbf{x}(t), \mathbf{u}(t), \mathbf{d}(t)) \in \mathbb{R}^6, \quad (1)$$

<sup>1</sup>The reference is denoted with \* symbol superscript, e.g.,  $\xi^*$ .

<sup>2</sup>The subscript  $dq$  is omitted for brevity, i.e., any generic variable  $\xi$  represents  $\xi_{dq}$ .

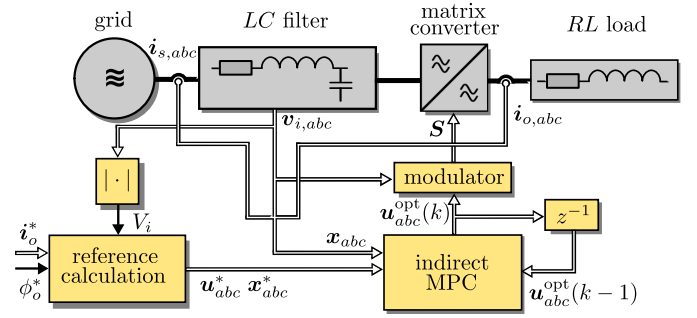


Fig. 2: Block diagram of the proposed indirect MPC scheme.

where the state vector  $\mathbf{x}(t)$  consists of the input source current  $\mathbf{i}_s(t)$ , input filter voltage  $\mathbf{v}_i(t)$ , and output current  $\mathbf{i}_o(t)$ , i.e., it is defined as

$$\mathbf{x}(t) = [\mathbf{i}_s^T(t) \quad \mathbf{v}_i^T(t) \quad \mathbf{i}_o^T(t)]^T \in \mathbb{R}^6.$$

Moreover, the converter voltage  $\mathbf{v}_o(t)$  is chosen as the control input  $\mathbf{u}(t)$ , i.e.,  $\mathbf{u}(t) = \mathbf{v}_o(t) \in \mathbb{R}^2$ , while the source (grid) voltage  $\mathbf{v}_s(t)$ —which is assumed to be constant—is treated as a disturbance  $\mathbf{d}(t)$ , i.e.,  $\mathbf{d}(t) = \mathbf{v}_s(t) \in \mathbb{R}^2$ .

The nonlinear dynamical system model of the MC with an LC input filter and an RL load is expressed as

$$\frac{d\mathbf{i}_s(t)}{dt} = \omega_i \mathbf{J} \mathbf{i}_s(t) - \frac{R_f}{L_f} \mathbf{i}_s(t) - \frac{1}{L_f} \mathbf{v}_i(t) + \frac{1}{L_f} \mathbf{v}_s(t) \quad (2a)$$

$$\frac{d\mathbf{v}_i(t)}{dt} = \omega_i \mathbf{J} \mathbf{v}_i(t) + \frac{1}{C_f} \mathbf{i}_s(t) - \frac{1}{C_f} \mathbf{i}_i(t) \quad (2b)$$

$$\frac{d\mathbf{i}_o(t)}{dt} = \omega_o \mathbf{J} \mathbf{i}_o(t) - \frac{R_l}{L_l} \mathbf{i}_o(t) + \frac{1}{L_l} \mathbf{v}_o(t), \quad (2c)$$

where  $\omega_i$  and  $\omega_o$  denote the angular frequencies of the input and output sides, respectively. The parameters  $R_f$ ,  $L_f$ , and  $C_f$  represent the resistance, inductance, and capacitance of the input filter, respectively. Moreover,  $R_l$  and  $L_l$  denote the load resistance and inductance, respectively. Finally, the converter input current  $\mathbf{i}_i(t)$  is defined as the input-state product

$$\mathbf{i}_i(t) = \frac{\mathbf{i}_o^T(t) \mathbf{v}_o(t)}{k \mathbf{v}_i(t) k^2} \mathbf{v}_i(t),$$

while  $\mathbf{J}$  is the rotation matrix

$$\mathbf{J} = \begin{bmatrix} 0 & 1 \\ 1 & 0 \end{bmatrix}.$$

### B. Reference Calculation

The reference point of the state  $\mathbf{x}(t)$  and control input  $\mathbf{u}(t)$  are computed based on the desired output current magnitude  $I_o(t)$  and the reference angle of the converter output voltage  $\phi_o(t)$ .

More specifically, starting with the desired state, the reference for the converter output current  $\mathbf{i}_o(t) = [i_{od}(t) \quad i_{oq}(t)]^T$  is chosen as

$$\mathbf{i}_o(t) = \begin{bmatrix} I_o(t) \\ 0 \end{bmatrix},$$

while the output voltage angle  $\phi_o(t)$  is defined as

$$\phi_o(t) = 2\pi f_o t,$$

where  $f_o$  is the desired output frequency.

The input source current reference  $\mathbf{i}_s(t) = [i_{sd}(t) \ i_{sq}(t)]^T$  is calculated using a power balance approach [19], while also considering the converter efficiency  $\eta$ . For simplicity, but without loss of generality, a unity power factor is assumed on the input side of the converter. Accordingly, the grid voltage and source current vectors are defined as  $\mathbf{v}_s(t) = [v_{sd}(t) \ v_{sq}(t)]^T = [V_s \ 0]^T$  and  $\mathbf{i}_s(t) = [I_s(t) \ 0]^T$ , where  $V_s$  and  $I_s$  denote the magnitudes of the source (grid) voltage and current, respectively.

Hence, considering the active power reference at the input side of the converter as

$$P_i(t) = \frac{3 I_s(t) V_s}{2} - \frac{3 I_s(t)^2 R_f}{2}, \quad (3)$$

where the second term accounts for the input filter losses, and the output-side active power reference as

$$P_o(t) = \frac{3 I_o(t)^2 R_l}{2}, \quad (4)$$

together with the converter efficiency

$$P_o(t) = \eta P_i(t), \quad (5)$$

the desired magnitude of the input source current can be obtained by solving (3)–(5) for  $I_s(t)$ , yielding

$$I_s(t) = \frac{V_s \eta + \sqrt{\eta \left( V_s^2 \eta - 4 I_o(t)^2 R_f R_l \right)}}{2 R_f \eta}. \quad (6)$$

Finally, the input-side filter voltage reference  $\mathbf{v}_i(t) = [v_{id}(t) \ v_{iq}(t)]^T$  is computed as

$$\begin{aligned} \mathbf{v}_i(t) &= \mathbf{v}_s(t) - (R_f \mathbf{I}_2 + \omega_i L_f \mathbf{J}) \mathbf{i}_s(t) \\ &= \begin{bmatrix} V_s & R_f I_s(t) \\ \omega_i L_f I_s(t) & 0 \end{bmatrix}, \end{aligned} \quad (7)$$

where  $\mathbf{I}_n$  denotes the identity matrix of size  $n$ .

As for the output voltage reference  $\mathbf{v}_o(t)$ , i.e., the desired control input, it is computed as

$$\begin{aligned} \mathbf{v}_o(t) &= (R_l \mathbf{I}_2 + \omega_o L_l \mathbf{J}) \mathbf{i}_o(t) \\ &= \begin{bmatrix} R_l i_{od}(t) & \omega_o L_l i_{oq}(t) \\ R_l i_{oq}(t) & \omega_o L_l i_{od}(t) \end{bmatrix}. \end{aligned} \quad (8)$$

### C. Linearization and Discretization

The nonlinear state-space model (1) is linearized around the reference point by computing the Jacobian matrices, resulting in the small-signal model:

$$\frac{d\Delta \mathbf{x}(t)}{dt} = \mathbf{A}_c \Delta \mathbf{x}(t) + \mathbf{B}_c \Delta \mathbf{u}(t) \quad (9a)$$

$$\Delta \mathbf{y}(t) = \mathbf{C}_c \Delta \mathbf{x}(t) \quad (9b)$$

where the output of the system is chosen as  $\mathbf{y}(t) = [\mathbf{v}_i^T(t) \ \mathbf{i}_o^T(t)]^T$ . Moreover, the system  $\mathbf{A}_c$ , input  $\mathbf{B}_c$ , and output  $\mathbf{C}_c$  matrices are defined as

$$\mathbf{A}_c = \begin{bmatrix} \frac{R_f}{L_f} & \omega_i & \frac{1}{L_f} & 0 & 0 & 0 \\ \omega_i & \frac{R_f}{L_f} & 0 & \frac{1}{L_f} & 0 & 0 \\ \frac{1}{C_f} & 0 & \mathbf{A}_{c33} & \mathbf{A}_{c34} & \mathbf{A}_{c35} & \mathbf{A}_{c36} \\ 0 & \frac{1}{C_f} & \mathbf{A}_{c43} & \mathbf{A}_{c44} & \mathbf{A}_{c45} & \mathbf{A}_{c46} \\ 0 & 0 & 0 & 0 & \frac{R_l}{L_l} & \omega_o \\ 0 & 0 & 0 & 0 & \omega_o & \frac{R_l}{L_l} \end{bmatrix}$$

$$\mathbf{B}_c = \begin{bmatrix} 0 & 0 \\ 0 & 0 \\ \mathbf{B}_{c31} & \mathbf{B}_{c32} \\ \mathbf{B}_{c41} & \mathbf{B}_{c42} \\ \frac{1}{L_l} & 0 \\ 0 & \frac{1}{L_l} \end{bmatrix} \quad \text{and} \quad \mathbf{C}_c = \begin{bmatrix} \mathbf{0}_4 & \mathbf{I}_2 & \mathbf{I}_4 \end{bmatrix}.$$

The detailed expressions for the time-varying entries in  $\mathbf{A}_c$  and  $\mathbf{B}_c$  are provided in Appendix A. Note that the small-signal variable represents the difference between the actual value and its reference, i.e.,  $\Delta \xi = \xi - \xi^*$ .

Following this, the continuous-time linear state-space model (9) is discretized using the forward Euler method, resulting in the discrete-time state-space representation

$$\Delta \mathbf{x}(k+1) = \mathbf{A}_d \Delta \mathbf{x}(k) + \mathbf{B}_d \Delta \mathbf{u}(k) \quad (10a)$$

$$\Delta \mathbf{y}(k) = \mathbf{C}_d \Delta \mathbf{x}(k), \quad (10b)$$

where the discrete-time matrices are  $\mathbf{A}_d = T_s \mathbf{A}_c + \mathbf{I}_6$  and  $\mathbf{B}_d = T_s \mathbf{B}_c$ , with  $T_s$  being the chosen sampling interval, and  $k \in \mathbb{N}$  indicating the discrete time step.

It is worth noting that, to reduce the computational burden during real-time implementation, the elements of  $\mathbf{A}_d$  and  $\mathbf{B}_d$  that are independent of the reference values can be computed offline and subsequently stored in look-up tables (LUTs) for use in real time.

### D. Indirect MPC as a Constrained QP

The discretized system in (10) serves as the prediction model for the proposed indirect MPC scheme, enabling the prediction of system evolution over a prediction horizon of  $N_p$  time steps. To evaluate the future performance of the system, the desired control objectives—namely, the accurate tracking of the output reference as well as the manipulation of the controller bandwidth—are incorporated into the following cost function:

$$J(k) = \sum_{l=k}^{k+N_p-1} k \mathbf{y}^*(l+1) - \mathbf{y}(l+1) \mathbf{k}_Q^2 + \lambda_u k \mathbf{u}(l) - \mathbf{u}(l-1) \mathbf{k}_2^2. \quad (11)$$

In (11), the weighting matrix  $\mathbf{Q}$  penalizes the output tracking errors at each step of the prediction horizon through the chosen weighting factors

$$\mathbf{Q} = \text{diag} \left( \frac{k_{vi}}{V_b^2}, \frac{k_{vi}}{V_b^2}, \frac{1}{I_b^2}, \frac{1}{I_b^2} \right).$$

Here,  $V_b = V_i$  denotes the nominal (base) peak phase-to-neutral input voltage, while  $I_b = 5\text{ A}$  is the nominal peak phase-to-neutral input current. The parameter  $k_{vi} > 0$  is a weighting factor that prioritizes the tracking of the two output variables. Finally, the weighting factor  $\lambda_u > 0$  determines the trade-off between the two control objectives by adjusting the penalty on the control effort term.

To find the sequence of optimal control increments  $\Delta \mathbf{U}^{\text{opt}}(k) = [\Delta \mathbf{u}^{\text{opt}^T}(k) \ \Delta \mathbf{u}^{\text{opt}^T}(k+1) \ \dots \ \Delta \mathbf{u}^{\text{opt}^T}(k+N_p-1)]^T \in \mathbb{R}^{2N_p}$  at each sampling interval  $T_s$ , the following optimization problem is solved in real time:

$$\underset{\Delta \mathbf{U}(k)}{\text{minimize}} \quad J(k) \quad (\text{see (11)}) \quad (12a)$$

$$\text{subject to} \quad \Delta \mathbf{x}(l+1) = \mathbf{A}_d \Delta \mathbf{x}(l) + \mathbf{B}_d \Delta \mathbf{u}(l) \quad (12b)$$

$$\Delta \mathbf{y}(l) = \mathbf{C}_d \Delta \mathbf{x}(l) \quad (12c)$$

$$k \mathbf{u}(l) k < \frac{\rho}{2} \frac{V_i}{3} \quad (12d)$$

$$8l = k, \dots, k+N_p-1.$$

To reformulate the optimization problem (12) into a standard quadratic programming (QP) form that can be solved efficiently using the adopted solver (see Section II-E), a procedure similar to that described in [20] is employed and in detail explained in Appendix B. In doing so, the cost function in (11) is expressed as

$$J(k) = \Delta \mathbf{U}(k)^T \mathbf{H}(k) \Delta \mathbf{U}(k) + 2 \boldsymbol{\Theta}(k)^T \Delta \mathbf{U}(k) + \theta(k), \quad (13)$$

where the time-varying Hessian matrix  $\mathbf{H}(k) \in \mathbb{R}^{2N_p \times 2N_p}$  is given by

$$\mathbf{H}(k) = \boldsymbol{\Upsilon}(k)^T \tilde{\mathbf{Q}} \boldsymbol{\Upsilon}(k) + \lambda_u \mathbf{S}^T \mathbf{S},$$

vector  $\boldsymbol{\Theta}(k) \in \mathbb{R}^{2N_p}$  is

$$\boldsymbol{\Theta}(k) = (\boldsymbol{\Upsilon}(k))^T \tilde{\mathbf{Q}} \boldsymbol{\Gamma}(k) \Delta \mathbf{x}(k) + \lambda_u \mathbf{S}^T \mathbf{K}(k),$$

and the time-varying scalar  $\theta(k)$  is

$$\theta(k) = k \boldsymbol{\Gamma}(k) \Delta \mathbf{x}(k) k_{\tilde{\mathbf{Q}}}^2 + \lambda_u k \mathbf{K}(k) k_2^2,$$

where matrices  $\boldsymbol{\Upsilon}(k)$ ,  $\boldsymbol{\Gamma}(k)$ ,  $\mathbf{K}(k)$ ,  $\tilde{\mathbf{Q}}$ ,  $\mathbf{S}$ , and  $\mathbf{E}$  can be found in Appendix B. Note that the vector  $\mathbf{K}(k)$  accounts for variations in the control input reference between the current and previous time steps, thereby improving the performance of the proposed MPC, particularly during transients, while also benefiting steady-state operation.

With cost function (13), and after omitting the scalar term  $\theta(k)$  since it does not affect the optimal solution, the proposed optimal control problem in a constrained QP form is given by

$$\underset{\Delta \mathbf{U}(k)}{\text{minimize}} \quad J(k) \quad (\text{see (13)}) \quad (14a)$$

$$\text{subject to} \quad k \Delta \mathbf{u}(l) + \mathbf{u}(l) k < \frac{\rho}{2} \frac{V_i}{3} \quad (14b)$$

$$8l = k, \dots, k+N_p-1.$$

Solving this QP provides the optimal sequence of control input increments over the prediction horizon in the  $dq$  reference frame. As per the receding horizon policy, only the first

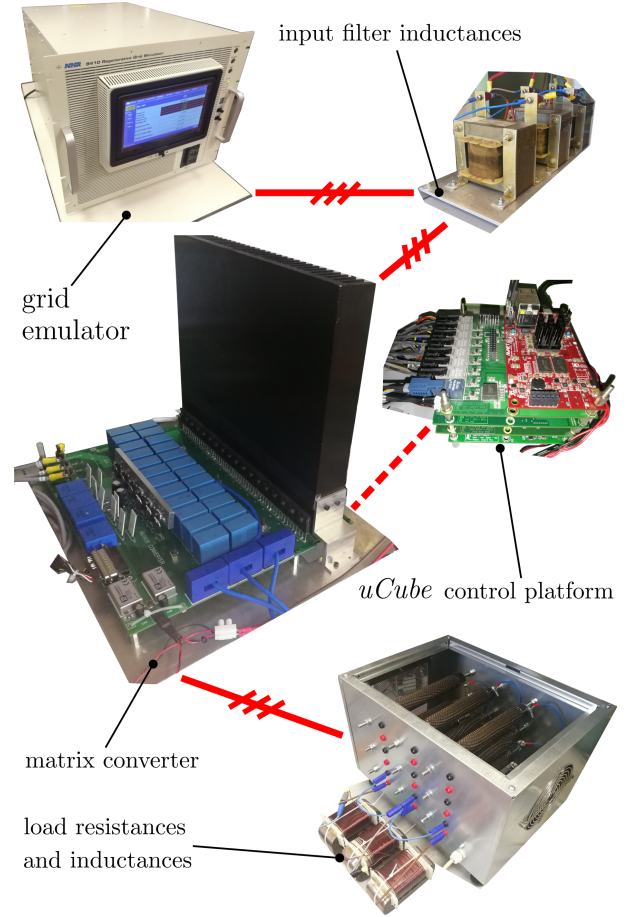


Fig. 3: The used experimental setup.

control increment is added to the desired control input, i.e.,  $\mathbf{u}^{\text{opt}}(k) = \mathbf{u}(k) + \Delta \mathbf{u}^{\text{opt}}(k)$ , and then  $\mathbf{u}^{\text{opt}}(k)$  is transformed into the three-phase ( $abc$ ) reference frame, yielding  $\mathbf{u}_{abc}^{\text{opt}}(k)$ . The resulting modulating signal is subsequently applied to the modulator to generate the switching signals for the converter, as illustrated in Fig. 2. The remaining control actions are discarded and the optimization procedure starts again in the next time step based on new measurements.

### E. Computationally-Efficient QP Solver

To solve the QP problem in (14), a gradient-based Barzilai–Borwein (BB) solver [21], similar to the approach in [22], is employed. The output constraint in (14b) can be interpreted as a set of  $N_p$  circles with radius  $\frac{\rho}{2} \frac{V_i}{3}$ . To handle this constraint, a projection method is adopted, as described in [23].

## III. EXPERIMENTAL RESULTS

The proposed control approach was experimentally validated using a custom-built test bench, shown in Fig. 3. The setup consists of a grid emulator, an input  $LC$  filter, a matrix converter, and an  $RL$  load. The corresponding system parameters are summarized in Table I. The indirect MPC scheme was implemented on a *uCube* control board [24] with a

TABLE I: System parameters

Parameters	Symbol	Value
Grid voltage (phase-to-neutral)	$V_i$	84 V
Grid angular frequency	$\omega_i$	$2\pi \times 50$ rad/s
Filter inductor	$L_f$	2.4 mH
Filter capacitor	$C_f$	12 $\mu$ F
Filter resistor	$R_f$	1.5 $\Omega$
Load angular frequency	$\omega_o$	$2\pi \times 60$ rad/s
Load resistor	$R_l$	12 $\Omega$
Load inductor	$L_l$	3.7 mH
Switching (sampling) frequency	$f_{sw}$ ( $f_{s\text{amp}}$ )	10 kHz

TABLE II: MPC and PI tuning parameters

$f_c$ [Hz]	MPC		PI	
	$\lambda_u$	$k_{vi}$	$k_P$	$k_I$
650	$1 \times 10^9$	$1 \times 10^5$	29.4947	$1.2891 \times 10^5$
600	$1 \times 10^9$	0.01	26.3028	$1.0984 \times 10^5$
500	$1 \times 10^9$	0.1	19.9190	$7.6276 \times 10^4$
450	$5 \times 10^5$	0.2	16.7271	$6.1784 \times 10^4$
400	$2 \times 10^4$	0.2	13.5352	$4.8817 \times 10^4$
380	$3.5 \times 10^4$	0.2	12.2584	$4.4057 \times 10^4$

prediction horizon of three time steps ( $N_p = 3$ ) and a sampling frequency of 10 kHz. This platform integrates current and voltage measurements as well as protection features. Finally, the board is equipped with a Xilinx Zynq-7000 system-on-chip (SoC).

As mentioned, in matrix converters, the controller bandwidth and maximum output power are competing objectives. This section experimentally investigates this trade-off by examining the maximum achievable output power for different controller bandwidths. Furthermore, to better assess the benefits of the discussed indirect MPC approach, comparisons with a linear PI-based controller are provided.

#### A. MPC Tuning Procedure

According to the MPC formulation presented in Section II-D, the chosen cost function includes two tunable parameters, i.e.,  $\lambda_u$  and  $k_{vi}$ . As mentioned,  $\lambda_u$  influences the controller bandwidth, while  $k_{vi}$  relates to the input voltage reference tracking and thus affects the suppression of input filter oscillations. By appropriately tuning these two weighting factors, a favorable balance between output power and controller bandwidth can be achieved.

#### B. PI Tuning Procedure

The PI controller is tuned with a pole placement approach. The controller gains are calculated as

$$\left. \begin{array}{l} k_P = 0 \\ k_I = \omega_n R_l \quad \omega_n^2 L_l \end{array} \right\} \text{ when } \omega_n < \frac{R_l}{2\zeta L_l}$$

and

$$\left. \begin{array}{l} k_P = 2\zeta\omega_n L_l \quad R_l \\ k_I = \omega_n^2 L_l \end{array} \right\} \text{ when } \omega_n > \frac{R_l}{2\zeta L_l}$$

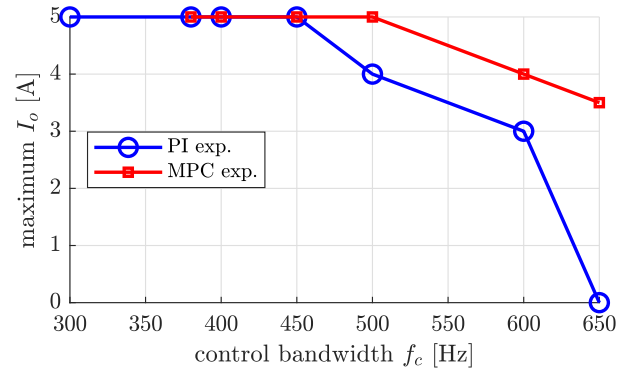


Fig. 4: Trade-off between converter maximum output current amplitude  $I_0$  and controller bandwidth  $f_c$ .

where  $\omega_n$  is the desired closed-loop bandwidth and  $\zeta$  denotes the damping.

#### C. Power Limit

To investigate the maximum output power achievable by the proposed indirect MPC scheme and the benchmark linear controller, both are tested across a range of controller bandwidths  $f_c$ . The controller parameters of both methods for the different operating points examined are listed in Table II. Note that during the tests, the maximum output current is limited to 5 A due to the constraints on the maximum output voltage.

Fig. 4 illustrates the maximum output power achieved by both controllers at various bandwidth frequencies. As observed, the indirect MPC consistently outperforms the PI-based controller as the controller bandwidth increases. This demonstrates the superior capability of MPC to achieve a more favorable trade-off between converter output power and controller bandwidth.

#### D. Time-Domain Results

In the following, the performance of both controllers is evaluated under steady-state and transient conditions, considering a controller bandwidth of  $f_c = 600$  Hz.

1) *Steady-State Performance*: First, the steady-state performance of the two controllers is assessed. The most relevant waveforms are shown in Fig. 5. It can be observed that the input quantities of the PI-based controller begin to exhibit slight distortion when the output current reaches 3 A, indicating that the system is operating near its stability limit. In contrast, the input current under the indirect MPC shows lower ripple levels, despite the converter delivering a higher output current of 4 A.

This difference is further highlighted by the normalized harmonic spectra of the phase- $a$  source current  $i_s(t)$ , presented in Fig. 6. The input current with the linear controller generally demonstrates higher harmonic distortion compared to MPC. Notably, a prominent harmonic at 650 Hz is observed, which is close to the resonance frequency of the  $LC$  input filter.

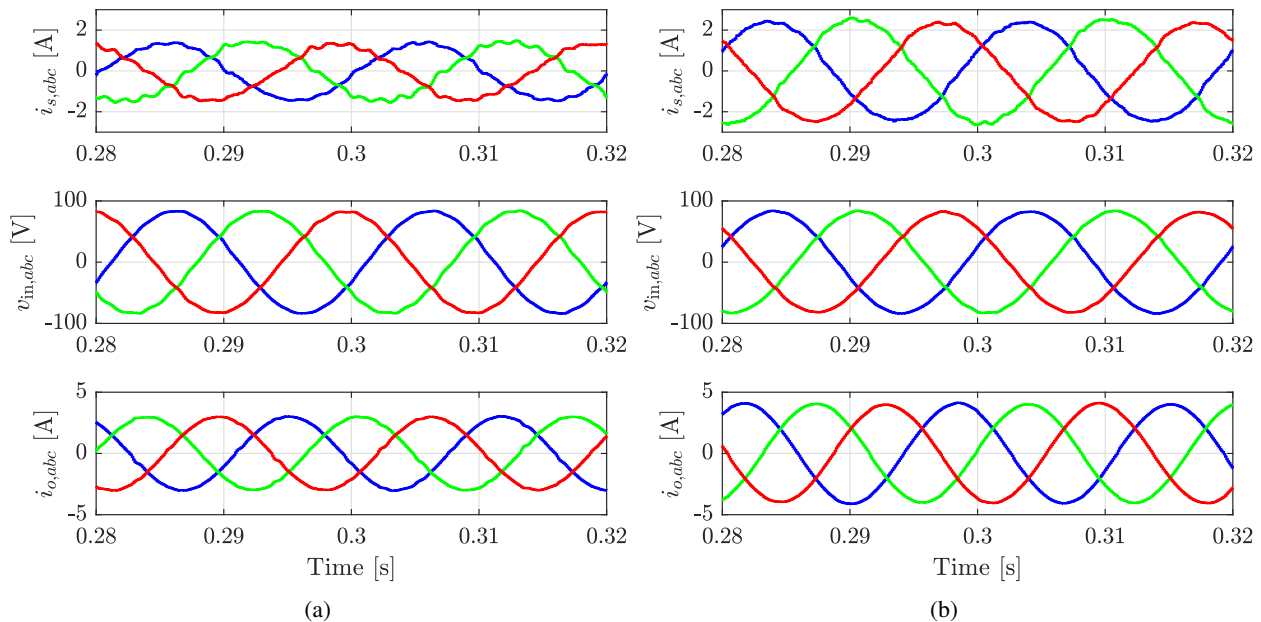


Fig. 5: Steady-state waveforms: (a) PI,  $I_o = 3$  A; (b) MPC,  $I_o = 4$  A.  $f_c = 600$  Hz.

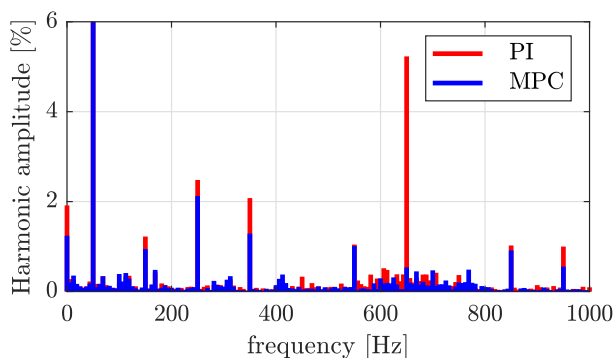


Fig. 6: Harmonic spectrum of  $i_s$  with PI-based and MPC-based control schemes at operating conditions shown in Fig. 5.

2) *Dynamic Performance*: Next, the dynamic performance of the controllers is examined. Fig. 7 shows the transient response to a step-up change in the  $d$ -component of the output current reference. As observed, the rise times of both MPC and PI controllers are very similar, confirming that both operate at the desired bandwidth frequency. However, the MPC exhibits a smaller overshoot compared to the PI controller.

3) *MPC Transient Response at Maximum Power*: In the final scenario, Fig. 8 illustrates the transient response of indirect MPC when the reference output current  $i_{od}(t)$  changes from 3 to 4 A. As observed, the controller effectively manages the change in operating point, even though the new point corresponds to the maximum achievable current at the considered controller bandwidth. Furthermore, the small oscillation in the  $d$ -axis current is rapidly attenuated within a few milliseconds.

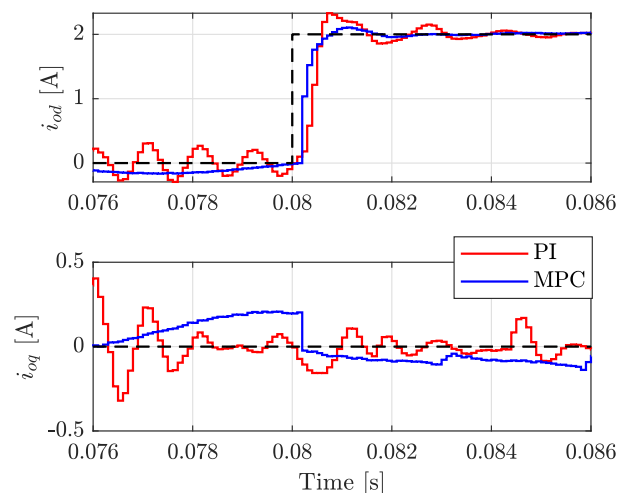


Fig. 7: Dynamic response of PI and MPC to a step-up change in  $i_{od}$  from 0 to 2 A at  $f_c = 600$  Hz.

#### E. Computational Burden

Finally, Fig. 9 shows the computation time of the proposed MPC strategy with  $N_p = 3$ , implemented on the Zynq ARM Cortex-A9 of the employed control platform. In the figure, the high-level voltage corresponds to the control computation period within the sampling interval  $T_s = 100 \mu\text{s}$ . As observed, the execution time is approximately  $50 \mu\text{s}$ , demonstrating the feasibility of real-time implementation of the proposed approach on industrial control hardware.

#### IV. CONCLUSION

This paper presented an indirect MPC strategy for a matrix converter with an input  $LC$  filter. Compared to conventional

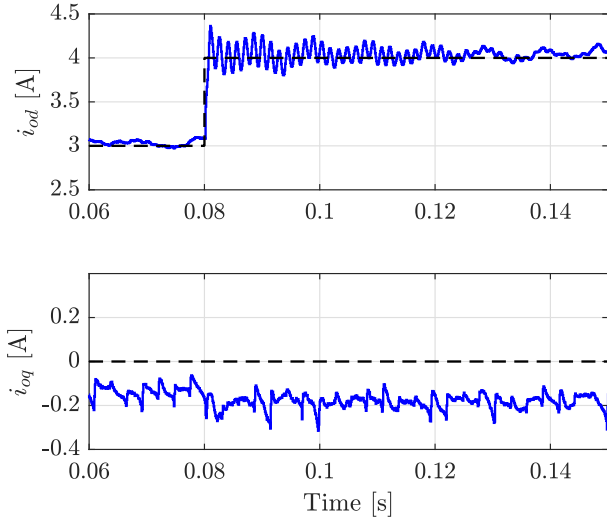


Fig. 8: Dynamic response of MPC to a step-up change in  $i_{od}$  from 3 to 4 A at  $f_c = 600$  Hz.

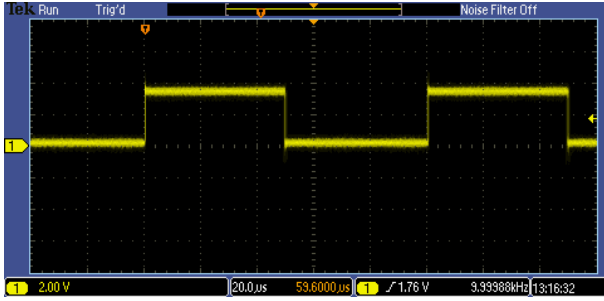


Fig. 9: Computation time of the proposed indirect MPC scheme.

PI-based controllers, the proposed approach offers a favorable trade-off between controller bandwidth and converter output power, enabling higher bandwidth and improved power handling. This improvement allows for a better utilization of the matrix converter hardware, making it particularly suitable for applications demanding fast dynamic responses, high power, and low current ripple. The presented experimental results validate both the performance advantages and the real-time feasibility of the proposed method.

#### APPENDIX A STATE-SPACE MODEL MATRICES

The matrix entries of  $A_c$  and  $B_c$  that require real-time computation as a result of the linearization process are given by

$$\begin{aligned} A_{c33} &= \frac{(v_{id}^2 \quad v_{iq}^2) (i_{od} v_{od} + i_{oq} v_{oq})}{C_f \sigma^2}, \\ A_{c34} &= \omega_i + \frac{2 v_{id} v_{iq} (i_{od} v_{od} + i_{oq} v_{oq})}{C_f \sigma^2}, \\ A_{c35} &= \frac{v_{id} v_{od}}{C_f \sigma}, \quad A_{c36} = \frac{v_{id} v_{oq}}{C_f \sigma}, \end{aligned}$$

$$A_{c43} = \omega_i + \frac{2 v_{id} v_{iq} (i_{od} v_{od} + i_{oq} v_{oq})}{C_f \sigma^2},$$

$$A_{c44} = \frac{(v_{id}^2 \quad v_{iq}^2) (i_{od} v_{od} + i_{oq} v_{oq})}{C_f \sigma^2},$$

$$A_{c45} = \frac{v_{iq} v_{od}}{C_f \sigma}, \quad A_{c46} = \frac{v_{iq} v_{oq}}{C_f \sigma},$$

$$B_{c31} = \frac{i_{od} v_{id}}{C_f \sigma}, \quad B_{c32} = \frac{i_{oq} v_{id}}{C_f \sigma},$$

$$B_{c41} = \frac{i_{od} v_{iq}}{C_f \sigma}, \quad \text{and} \quad B_{c42} = \frac{i_{oq} v_{iq}}{C_f \sigma},$$

where

$$\sigma = (v_{id}^2 + v_{iq}^2).$$

#### APPENDIX B DERIVATION OF QP COST FUNCTION

The first term of the cost function in (11) is reformulated as

$$\begin{aligned} J_1(k) &= \sum_{l=k}^{k+N_p-1} k \mathbf{y}(l+1)^T \mathbf{y}(l+1) \mathbf{K}_Q^2 \\ &= \sum_{l=k}^{k+N_p-1} k \Delta \mathbf{y}(l+1)^T \mathbf{K}_Q^2 \\ &= \sum_{l=k}^{k+N_p-1} (\Delta \mathbf{y}(l+1))^T \mathbf{Q} \Delta \mathbf{y}(l+1) \\ &= (\Delta \mathbf{Y}(k))^T \tilde{\mathbf{Q}} \Delta \mathbf{Y}(k) \\ &= k \Gamma(k) \Delta \mathbf{x}(k) + \Upsilon(k) \Delta \mathbf{U}(k) \mathbf{K}_Q^2, \end{aligned} \quad (15)$$

where the output trajectory is defined as

$$\Delta \mathbf{Y}(k) = \Gamma(k) \Delta \mathbf{x}(k) + \Upsilon(k) \Delta \mathbf{U}(k),$$

and the block diagonal penalty matrix  $\tilde{\mathbf{Q}} \in \mathbb{R}^{4N_p \times 4N_p}$  is defined as

$$\tilde{\mathbf{Q}} = \text{diag}(\mathbf{Q}, \dots, \mathbf{Q}).$$

Matrices  $\Gamma(k) \in \mathbb{R}^{4N_p \times 6}$ ,  $\Upsilon(k) \in \mathbb{R}^{4N_p \times 2N_p}$  share a similar structure to those presented in [20]. The key difference lies in the fact that the proposed MPC scheme is formulated in the  $dq$ —instead of the  $\alpha\beta$ —reference frame. Furthermore, due to the linearization process, the state matrix  $A_d(k)$  and input matrix  $B_d(k)$  are time-varying and must be updated in real time. For a prediction horizon of three steps ( $N_p = 3$ ), the corresponding matrices in (15) are given by

$$\begin{aligned} \Gamma(k) &= \begin{bmatrix} C_d A_d(k) \\ C_d (A_d(k))^2 \\ C_d (A_d(k))^3 \end{bmatrix}, \\ \Upsilon(k) &= \begin{bmatrix} C_d B_d(k) & \mathbf{0}_{4 \times 2} & \mathbf{0}_{4 \times 2} \\ C_d A_d(k) B_d(k) & C_d B_d(k) & \mathbf{0}_{4 \times 2} \\ C_d (A_d(k))^2 B_d(k) & C_d A_d(k) B_d(k) & C_d B_d(k) \end{bmatrix}. \end{aligned}$$

The second term of the cost function in (11) is reformulated as

$$\begin{aligned}
J_2(k) &= \sum_{l=k}^{k+N_p-1} \lambda_u k \mathbf{u}(l) \mathbf{u}(l-1) k_2^2 \\
&= \sum_{l=k}^{k+N_p-1} \lambda_u k \Delta \mathbf{u}(l) \Delta \mathbf{u}(l-1) + \mathbf{u}(l) \mathbf{u}(l-1) k_2^2 \\
&= \lambda_u k \mathbf{S} \Delta \mathbf{U}(k) + \mathbf{K}(k) k_2^2,
\end{aligned} \tag{16}$$

with

$$\mathbf{S} = \begin{bmatrix} \mathbf{I}_2 & \mathbf{0}_{2 \times 2} & \mathbf{0}_{2 \times 2} \\ \mathbf{I}_2 & \mathbf{I}_2 & \mathbf{0}_{2 \times 2} \\ \mathbf{0}_{2 \times 2} & \mathbf{I}_2 & \mathbf{I}_2 \end{bmatrix}.$$

The time-varying vector  $\mathbf{K}(k)$  is introduced to account for changes in the control input reference. This is defined as

$$\mathbf{K}(k) = \mathbf{E} \Delta \mathbf{u}(k-1) + \begin{bmatrix} \mathbf{u}(k) & \mathbf{u}(k-1) \\ \mathbf{u}(k+1) & \mathbf{u}(k) \\ \mathbf{u}(k+2) & \mathbf{u}(k+1) \end{bmatrix},$$

where

$$\mathbf{E} = \begin{bmatrix} \mathbf{I}_2 \\ \mathbf{0}_{2 \times 2} \\ \mathbf{0}_{2 \times 2} \end{bmatrix}.$$

Assuming a step reference change is applied at time step  $k$ , control input reference  $\mathbf{u}(l)$  for  $l = k, k+1, \dots, k+N_p-1$  changes only between time steps  $k-1$  and  $k$ , while it remains constant within the prediction horizon. Under this condition,  $\mathbf{K}(k)$  simplifies to

$$\mathbf{K}(k) = \mathbf{E} \Delta \mathbf{u}(k-1) + \begin{bmatrix} \mathbf{u}(k) & \mathbf{u}(k-1) \\ \mathbf{0}_{2 \times 1} \\ \mathbf{0}_{2 \times 1} \end{bmatrix}.$$

Therefore, by adding terms (15) and (16), the cost function  $J(k)$  is obtained in vector notation. This form is finally rearranged into a standard QP structure, as explained in [20], and presented in (13).

## REFERENCES

- [1] J. W. Kolar, T. Friedli, J. Rodriguez, and P. W. Wheeler, "Review of three-phase PWM ac-ac converter topologies," *IEEE Trans. Ind. Electron.*, vol. 58, no. 11, pp. 4988–5006, Nov. 2011.
- [2] S. Pipolo et al., "A novel matrix converter modulation with reduced number of commutations," *IEEE Trans. Ind. Appl.*, vol. 57, no. 5, pp. 4991–5000, Sep./Oct. 2021.
- [3] P. W. Wheeler, J. Rodriguez, J. C. Clare, L. Empringham, and A. Weinstein, "Matrix converters: A technology review," *IEEE Trans. Ind. Electron.*, vol. 49, no. 2, pp. 276–288, Apr. 2002.
- [4] L. Zarri, "Control of matrix converters," Ph.D. dissertation, University of Bologna, Bologna, Italy, 2007.
- [5] R. Cardenas et al., "Stability analysis of a wind energy conversion system based on a doubly fed induction generator fed by a matrix converter," *IEEE Trans. Ind. Electron.*, vol. 56, no. 10, pp. 4194–4206, Oct. 2009.
- [6] F. Liu, C. Klumpner, and F. Blaabjerg, "Stability analysis and experimental evaluation of a matrix converter drive system," in *Proc. IEEE Ind. Electron. Conf.*, Roanoke, VA, USA, Nov. 2003, pp. 2059–2065.
- [7] Y. Sun, M. Su, X. Li, H. Wang, and W. Gui, "A general constructive approach to matrix converter stabilization," *IEEE Trans. Power Electron.*, vol. 28, no. 1, pp. 418–431, Jan. 2013.
- [8] D. Casadei et al., "Large-signal model for the stability analysis of matrix converters," *IEEE Trans. Ind. Electron.*, vol. 54, no. 2, pp. 939–950, Apr. 2007.
- [9] J. M. Maciejowski, *Predictive Control With Constraints*, Prentice Hall, Englewood Cliffs, NJ, USA, 2002.
- [10] S. A. Odhano, A. Formentini, P. Zanchetta, R. Bojoi, and A. Tenconi, "Finite control set and modulated model predictive flux and current control for induction motor drives," in *Proc. IEEE Ind. Electron. Conf.*, Florence, Italy, Oct. 2016, pp. 2796–2801.
- [11] R. Rabbeni et al., "Finite states modulated model predictive control for active power filtering systems," in *Proc. IEEE Energy Convers. Congr. Expo.*, Montreal, QC, Canada, Oct. 2015, pp. 1556–1562.
- [12] J. Rodriguez, M. Rivera, J. W. Kolar, and P. W. Wheeler, "A review of control and modulation methods for matrix converters," *IEEE Trans. Ind. Electron.*, vol. 59, no. 1, pp. 58–70, Jan. 2012.
- [13] M. Rivera et al., "Review of predictive control methods to improve the input current of an indirect matrix converter," *IET Power Electron.*, vol. 7, no. 4, pp. 886–894, Apr. 2014.
- [14] M. Siami, D. Arab Khaburi, and J. Rodriguez, "Simplified finite control set-model predictive control for matrix converter-fed PMSM drives," *IEEE Trans. Power Electron.*, vol. 33, no. 3, pp. 2438–2446, Mar. 2018.
- [15] M. Rivera et al., "Predictive current control with input filter resonance mitigation for a direct matrix converter," *IEEE Trans. Ind. Electron.*, vol. 26, no. 10, pp. 2794–2803, Oct. 2011.
- [16] M. Vijayagopal et al., "Control of a direct matrix converter with modulated model-predictive control," *IEEE Trans. Ind. Appl.*, vol. 53, no. 3, pp. 2342–2349, May/Jun. 2017.
- [17] P. Karamanakos, E. Liegmann, T. Geyer, and R. Kennel, "Model predictive control of power electronic systems: Methods, results, and challenges," *IEEE Open J. Ind. Appl.*, vol. 1, pp. 95–114, 2020.
- [18] J. Rodriguez, J. Espinoza, M. Rivera, F. Villarroel, and C. Rojas, "Predictive control of source and load currents in a direct matrix converter," in *Proc. IEEE Int. Conf. Ind. Technol.*, Via del Mar, Chile, Mar. 2010, pp. 1826–1831.
- [19] M. Rivera et al., "Imposed sinusoidal source and load currents for an indirect matrix converter," *IEEE Trans. Ind. Electron.*, vol. 59, no. 9, pp. 3427–3435, Sep. 2012.
- [20] T. Geyer and D. E. Quevedo, "Multistep finite control set model predictive control for power electronics," *IEEE Trans. Power Electron.*, vol. 29, no. 12, pp. 6836–6846, Dec. 2014.
- [21] J. Barzilai and J. M. Borwein, "Two-point step size gradient methods," *IMA J. Numer. Anal.*, vol. 8, no. 1, pp. 141–148, Jan. 1988.
- [22] Q. Yang et al., "Computationally efficient fixed switching frequency direct model predictive control," *IEEE Trans. Power Electron.*, vol. 37, no. 3, pp. 2761–2777, Mar. 2022.
- [23] J. Nocedal and S. J. Wright, *Numerical Optimization*, 2nd ed. New York, NY, USA: Springer, 2006.
- [24] A. Galassini et al., "uCube: Control platform for power electronics," in *Proc. IEEE Workshop on Elect. Mach. Design, Control and Diagn.*, Nottingham, UK, Apr. 2017, pp. 216–221.